### Title

Overhauser dynamic nuclear polarization-enhanced NMR relaxometry




### Authors

Franck, John M
Kausik, Ravinath
Han, Songi



### Publication Date

2013-09-01

### DOI

10.1016/j.micromeso.2013.04.019

Peer reviewed

Published in final edited form as:
*Microporous Mesoporous Mater*. 2013 September 15; 178: 113–118. doi:10.1016/j.micromeso.2013.04.019.

# Overhauser Dynamic Nuclear Polarization-Enhanced NMR Relaxometry

**John M. Franck**, **Ravinath Kausik**, and **Songi Han**
Department of Chemistry and Biochemistry, University of California, Santa Barbara

## Abstract

We present a new methodological basis for selectively illuminating a dilute population of fluid within a porous medium. Specifically, transport in porous materials can be analyzed by now-standard nuclear magnetic resonance (NMR) relaxometry and NMR pulsed field gradient (PFG) diffusometry methods in combination with with the prominent NMR signal amplification tool, dynamic nuclear polarization (DNP). The key components of the approach introduced here are (1) to selectively place intrinsic or extrinsic paramagnetic probes at the site or local volume of interest within the sample, (2) to amplify the signal from the local solvent around the paramagnetic probes with Overhauser DNP, which is performed *in situ* and under ambient conditions, and (3) to observe the ODNP-enhanced solvent signal with 1D or 2D NMR relaxometry methods, thus selectively amplifying only the relaxation dynamics of the fluid that resides in or percolates through the local porous volume that contains the paramagnetic probe. Here, we demonstrate the proof of principle of this approach by selectively amplifying the NMR signal of only one solvent population, which is in contact with a paramagnetic probe and occluded from a second solvent population. An apparent one-component $T_2$ relaxation decay is shown to actually contain two distinct solvent populations. The approach outlined here should be universally applicable to a wide range of other 1D and 2D relaxometry and PFG diffusometry measurements, including $T_1$–$T_2$ or $T_1$-$D$ correlation maps, where the occluded population containing the paramagnetic probes can be selectively amplified for its enhanced characterization.

### Keywords

Dynamic Nuclear Polarization; diffusion; NMR; T1; T2

## Introduction

Transport of fluids within porous materials offers important insight to their structure at the nm-mm length scale. Interestingly, in biology, transport from one location of the cell to another necessarily requires the passage through and around complex “blockades” of macromolecules, membranes, and structural elements that fill the cytoplasm, making the study of flow in these systems even more interesting and complex [1]. Similarly, synthetic materials are often designed with particular transport properties in mind, where the rate and pattern with which fluids transport from one region to another frequently defines the characteristic function of porous materials. To name a few notable examples, the analysis of

pore sizes and transport between pores in rocks has proven to be an important tool for identifying and characterizing underground reservoirs [2, 3, 4], while the transport of protons through nafion and other polymer electrolyte membranes is both long-debated and integral to the function of these materials, which offer great promise for the future of clean energy [5, 6, 7]. More generally, through scenarios like those illustrated in fig. 1, a relatively dilute portion of the porous sample can play an exceedingly important role. In a cell, this might be an organelle or a protein population in the cytoplasm occluded from the extracellular fluid or vice versa; in a catalytic substrate, this might represent small reactive pores, or as in polymer electrolyte membranes, this might correspond to the relatively few pores that permit complete transport of protons [8]. Thus, a minority and somewhat occluded porous population can often play a key functional role, whose explicit detection would be of great interest. It is clear that deeper insight to the complex transport patterns in materials will offer powerful new insights into their microstructure and function, in particular if one can target minority populations with distinct transport characteristics. Yet, in realistic systems, attempts to rationalize a porous structure-transport-property relation have often proven elusive.

Powerful experimental approaches exist, including light microscopy, surface characterization techniques and light scattering-based methods, but apply to porous materials only with great difficulty. Technologically relevant porous materials and systems often operate under high pressure, or are present at high opacity or viscosity, or display large susceptibility and permeability mismatches. Clearly, studies of intact materials under operating conditions can prove difficult.

Fortunately, nuclear magnetic resonance (NMR) based methods offer unique opportunities for the *in situ*, non-invasive, and tracer-less characterization of transport and flow in porous systems. NMR-based methods are attractive because they uniquely locate and track the displacements of nuclear centers of the solvent of interest. Thus, they characterize the transport of the fluids themselves, such as water *in situ* [9], while other methods might require the addition of a fluorophore or other external tracer particle. In contrast to the limitation of other methods, NMR-based methods are mainly limited by a need for higher sensitivity and signal contrast. Since rationalizing transport through percolated microstructures requires the ability to analyze signals coming from exceedingly dilute portions of the sample against a background of large signal amplitudes, overcoming the sensitivity limitation is of particular importance. At the same time, NMR requires a means of signal contrast, *i.e.* a means for resolving the signal from the dilute portion from the signal from the large background.

Field gradients can frequency-label the NMR signal of water molecules according to their position in space. This strategy for achieving signal contrast has allowed imaging, velocity, and diffusion studies, and even the generalized q-space imaging of transport [10]. However, one must apply very strong field gradients in order to achieve high spatial resolution, which also leads to less available NMR signal amplitudes per voxel. While NMR images of single cells [11] have been acquired and resolutions as low as one micron have been achieved [12, 13], such studies still represent values close to the technical limitation of the instrumentation. In other cases, NMR can resolve different chemical shifts for protons in different locations, and the use of NMR to track chemical exchange processes is very common, but such measurements require high-field high-resolution spectrometers, and their applicability is limited to systems where nuclei exchange between two different environments with very different chemical shifts. Especially for the study of fluid transport in porous system, this requirement is difficult to meet, as the solvent $^{1}$H NMR chemical shift will not sufficiently change as a function of pore size. Thus, to observe transport between

two populations of water, NMR requires alternative and better means of resolving the signal arising from the different populations of water than currently available.

Over more recent years, a unique NMR methodology that identifies spins based solely on their relaxation or diffusion properties has evolved [14, 15, 16, 17]. This method does not require high fields and can function even in environments which, due to instrumentation limitations or susceptibility mismatch, exhibit very inhomogeneous fields. In contrast to NMR imaging and chemical exchange techniques that make use of NMR spectroscopic signal and resolve signals that oscillate differently, this method achieves resolution of different water populations by observing the rate of decay of the NMR signal, due either to the transverse relaxation, the longitudinal relaxation ($T_1$), or the diffusion-induced decoherence ($D$)However, the problem of resolving signals that decay at different rates is mathematically ill-determined and becomes particularly problematic if the populations begin to approach the level of the noise [18]. This is unfortunate, since, as previously pointed out, the most interesting components of a system can occur in relatively small regions out of the overall whole. Here, DNP offers the opportunity to provide means for selectively enhancing such small signals in the presence of a large background signal of the bulk fluid.

DNP is a technique that permits the transfer of the relatively large electron spin polarization from an ESR (electron spin resonance) –active unpaired electron spin radical to the spins of nearby NMR-active nuclei. By selectively locating the radical-bearing molecules (*i.e.* the “spin labels”), which are typically TEMPO (*i.e.*, (2,2,6,6-Tetramethylpiperidin-1-yl)oxyl) derivatives, at a particular site, NMR signal at a select location can be amplified. For instance, this capability was recently demonstrated with solid state DNP by selectively enhancing the NMR signal from natural abundance $^{13}C$ nuclei in phenol or imidazolium groups attached to the surface of a nanoporous silica framework. This was achieved by adding an aqueous solution of the paramagnetic radical TEMPO to the sample, then saturating the electron spins of TEMPO with microwaves [19]. This demonstration represents the advent of a general technique that could be employed in solid-state magic angle spinning NMR, where chemical resolution, high fields, and isotopic labeling are feasible.

Here, we develop a similar technique that provides site resolution through the resolution and selective amplification of relaxation populations in systems with limited diffusion between different populations of water. Importantly, we rely on the Overhauser mechanism for DNP (ODNP), which operates under liquid-state conditions, and requires only very small sample quantities (3.5 μL). ODNP can efficiently amplify the NMR signal of water at ambient conditions and 0.35 T, a field which permits simultaneous analysis by X-band ESR line shape analysis, and is easily achieved with room temperature electromagnets or permanent magnets [20]. ODNP enhancements have been shown capable of measuring the local diffusivity of water within (sub-) nanometer distances of spin labels [21]. ODNP-derived hyperpolarized water signal was also employed as an authentic contrast agent in a room temperature imaging experiment to visualize flow through porous material [22], as well as more recently through veins and the blood brain barrier of *in vivo* rat models [23]. In the methodology presented here, ODNP selectively amplifies and provides contrast for a relaxation component that would otherwise remain invisible or difficult to detect.

In this communication, we present proof of principle experiments that rely on an experimental design involving three steps. First, a spin label – typically a TEMPO-based label – is selectively incorporated into the fluid of one type of compartment, pore, or otherwise occluded population of the sample. Alternatively, as discussed later, an intrinsically present spin label could be identified. Second, the typical Carr Purcell Meibloom Gill (CPMG) relaxation sequence measures the $T_2$ decay of the NMR signal.

Third, microwaves are applied to saturate the ESR transition of the spin label, and the CPMG-derived signal is acquired again. The compartments/pores containing the spin label are selectively enhanced, thus amplifying the signal arising from those compartments and providing clearer resolution of the different relaxation components.

## 2. Experimental

To demonstrate this procedure, a phantom was constructed as shown in fig. 2. A 0.6 mm i.d. 0.84 mm o.d. quartz capillary tube, which fits into the exact hardware configuration used in other ODNP experiments [21], was flame sealed in the center, loaded with 2.6 μL of water one one side of the tube, and 0.44 μL of 100 mM 4-hydroxy-TEMPO in water was loaded into the other. The two liquid chambers are completely isolated from each other. The 2.6 μL of pure water models a less interesting bulk background signal, while the 0.44 μL chamber where the 4-hydroxy-TEMPO probes have been incorporated models a smaller, occluded volume of fluid in a porous system, whose contribution to the signal we wish to enhance.

To achieve this enhancement, approximately 2.5 mW of microwave power irradiates the sample to partially saturate the electron spin transition. While the hardware can deliver up to 20 Watts of power, we chose 2.5 mW for illustration purposes as the dielectric cavity we employ has a high Q factor of 4,000 and so that this power yields similar amplitudes for the un-enhanced pure water signal and the enhanced signal from the 4-hydroxy-TEMPO solution. The general form of the sequence presented here can employ a range of microwave powers along an indirect “second” dimension, as shown in fig. 2, yielding datasets similar to fig. 4. The signal was excited and allowed to undergo transverse relaxation (*i.e.* $T_2$) decay during a standard CPMG sequence (fig. 2). For each echo, the main signal peak was selected from the Fourier transform of the time-domain signal.

In order to generate a real-valued signal decay for the $T_2$ curve, the resulting signal amplitudes needed to be correctly phased. Typically, the signal decay could be phased by noting that it always consists of real and positive values. However, since ODNP-enhanced signal is inverted in sign relative to the unenhanced signal, the signal decay – while entirely real – can take on either positive or negative values. Therefore, in order to phase this signal, the processing code adjusts the overall phase, ', of the signal to maximize the success function, $C$, which is

$$C=\frac{\sum_i \Re\{e^{i\varphi} s(t_i)\}^2}{\sum_i \Im\{e^{i\varphi} s(t_i)\}^2}, \quad (1)$$

where $s(t_i)$ is the echo amplitude of the CPMG signals at the different echo times, $t_i$. This correction yields entirely real-valued signal, with the imaginary component at noise levels for most points.

## 3. Results + Discussion

Fig. 3 presents both the signal where microwave irradiation turns on the ODNP enhancement effect, as well as the signal where the enhancement is turned off. In both cases, the 4-hydroxy-TEMPO probe molecules in the smaller (0.44 μL) chamber cause the NMR signal to decohere (*i.e.* decay) more rapidly – *i.e.* the water molecules in the smaller chamber contribute a signal with a shorter apparent $T_2$ time. Thus, the selective inclusion of free radical probes into one chamber of the phantom allows one to use NMR relaxometry techniques to separate the signal contributions arising from the two different chambers, even

though they do not exhibit distinguishable chemical shifts. Specifically, we do this by fitting the $T_2$ decay curves.

First, we analyze the signal acquired with the microwave saturation turned off by fitting the CPMG signal decay to a bi-exponential function.[1] We normalize the signal amplitude against the (best fit) amplitude of the signal at time 0. We can assign the slowly decaying component, with $T_2$ = 1.7 s (relative to a noise level of 0.017), to the signal from the chamber containing pure water and the rapidly decaying component, with $T_2$ = 36 ms and normalized amplitude 0.42, to the signal from the chamber containing the 100 mM 4-hydroxy-TEMPO. For pure water, without a second chamber, we measured a $T_2$ of 1.9 s Clearly, the $T_2$ value differs from that of pure water and the normalized amplitudes differ significantly from the actual ratio of the volumes in the two chambers, indicating that the quantification of the amplitudes and relaxation rates extracted from this bi-exponential fit is inexact. This may be related to the fact that the fast-relaxing component is highly dependent on the first few echo points, which may present small oscillating imperfections due to $B_1$ or static field inhomogeneities [24]. In order to better resolve the two components, and in particular better characterize the (spin-) dynamics of the fast relaxation component, one can turn on the microwave saturation for selective ODNP amplification.

As a result of selective ODNP enhancement, we observe a CPMG signal (fig. 3, bottom) that passes through zero and flips sign before finally decaying and remaining at zero amplitude. Such behavior differs from any conventional CPMG curve that presents a decay of signal from an equilibrium polarization state. The zero-crossing arises directly from the unique nature of ODNP, which hyperpolarizes and inverts the magnetization of the water molecules in the chamber containing the 4-hydroxy-TEMPO, and, as shown by fig. 3, provides additional contrast between the two relaxation components – *i.e.* additional contrast between the signals from the water in the two chambers. Furthermore, while the slow-relaxing component, now with $T_2$ = 1.9 s maintains a low amplitude of 0.55 (normalized against the amplitude of the previous, unenhanced experiment at time 0), the fast-relaxing component, with $T_2$ = 21 ms, achieves a greatly enhanced and inverted amplitude of −10.2. Clearly, ODNP amplifies the latter signal from the minority population to well above the noise level for this experiment, which is 0.011.

In summary, we note that in this idealized model system, the two populations of water remain physically separated throughout the experiment, and yet the apparent $T_2$ signal decay does not present the two signal populations with complete unambiguity until the ODNP effect is turned on. Further, we have shown that even if the $T_2$ decay is correctly assumed as two-component, we may not obtain accurate or even sensible fits. By removing this ambiguity, ODNP offers exciting prospects for analyzing fluid transport and solvent dynamics of occluded fluid volumes in complex systems with enhanced sensitivity. For instance, in the vesicle sample schematically represented in fig. 1, the specific localization of the radical-based spin probes within an occluded or slowly exchanging fluid population will allow for its unambiguous detection, even though the occluded population might be much smaller than the bulk fluid population.

## 4. Outlook

Future applications will target systems that involve some level of transport between the probe-containing, occluded fluid and the bulk fluid. For instance, the vesicle system pictured on the left of fig. 1, water passes through the semipermeable membrane at a limited rate. We

[1]Since the first 4 points of the fit residual show a transient oscillation (cf. [24]), we eliminate these points before fitting. This gives more reasonable values for the noise that we quote, but does not have a dramatic effect on the resulting fit.

present a simple analytical model for the ODNP enhancements in such systems, to aid in understanding and selecting future targets for this methodology. Here, we develop a model for ODNP in a system with transport between two populations with different $T_1$ rates. Specifically, from the seminal work of Hausser and Stehlik [25], as well as more recent work [26], we can deduce a differential equation for the enhancements of the two populations:

$$\frac{d}{dt}\begin{bmatrix} E_{\text{insides}}/x \\ E_{\text{bulk}} \end{bmatrix} = \begin{bmatrix} -k_\rho C_{SL}/x - T_{1,0}^{-1}/x - \Phi/\upsilon & \Phi/\upsilon \\ \Phi/\upsilon & -T_{1,0}^{-1}/x - \Phi/\upsilon \end{bmatrix} \begin{bmatrix} E_{\text{insides}}/x \\ E_{\text{bulk}} \end{bmatrix} + \begin{bmatrix} k_\rho C_{SL}/x + T_{1,0}^{-1}/x - k_\sigma s(659.3) C_{SL}/x \\ T_{1,0}^{-1} \end{bmatrix} \quad (2)$$

where $x$ is the mole ratio of the amount of "bulk" water to that of water "inside" the vesicles or occluded pores; $C_{SL}$ is the concentration of the spin label of the "inside" water population; $k_\rho C_{SL}$ and $k_\sigma C_{SL}$ are the rates of NMR self-relaxation induced by the spin label and of electron-nuclear cross-relaxation induced by the spin label, respectively; $T_{1,0}$ is the time constant for the background NMR relaxation processes; $\Phi$ is the flux of fluid molecules between the two populations, in units of moles; and $\upsilon$ is the total number of moles of fluid in the sample.[2] The eigenvalues provide the two decay rates that would appear in a bi-exponential analysis of $T_1$, while the steady-state solution quantifies the two ODNP enhancement factors for the occluded "inner" volume of water and the bulk water. With this model one could use the observed decay rates and ODNP signal enhancements to determine the flux $\Phi$, in addition to the standard ODNP parameters $k_\rho$ and $k_\sigma$, which would offer insight to a wide range of systems.

Many interesting systems, both naturally occurring or specifically designed, have an occluded population of fluid that could be analyzed in detail with this methodology. A TEMPO spin label can be covalently attached to the surfaces and interiors of proteins [27, 28], to various positions inside lipid membranes [29, 30], and to specific segments on synthetic polymers [31]. Additionally, one can localize freely dissolved spin labels in specific portions of porous media. can be encapsulated within lipid vesicles for extended periods of time (~hrs) [32]Lipid vesicles that could be prepared with vectorially aligned, spin labeled membrane proteins (for instance, the proteorhodopsin protein, studied by our lab and others has this capability), as well as the previously mentioned nafion membranes, which can form an ESR-active triplet state upon photoexcitation (as has been recently characterized [33]) also provide potentially intriguing targets. Such studies would permit analysis not only of the local translational dynamics of the spin label, but also of the timescale it takes for the enhanced signal from the hydration water near specially positioned electron spin to exchange and transport across the lipid membrane. These systems offer the opportunity to demonstrate resolution of different sites by ODNP enhancement, and select characterization via their $T_1$ or $T_2$ relaxation properties.

## 5. Conclusion

In this work, we have demonstrated a means for employing Overhauser Dynamic Nuclear Polarization (ODNP) to selectively amplify an otherwise small contribution to the NMR signal decay, thus allowing one to better resolve different contributions to the NMR relaxation decay or diffusion coefficients, and so to better resolve isolated populations of fluids in a porous material that may turn out to be critical. An important benefit of the EPR and ODNP approach is that there is, in principle, no limit to the size and complexity of the system to be studied, as long as spin probes can be strategically introduced. by combining with other NMR techniques, it should be possible both to add a $T_1$ dimension to the

[2] *i.e.* $\Phi/\upsilon$ gives the flux of spin signal as a fraction of the total NMR signal

experiment presented here, or to repeat this experiment in a constant field gradient with different echo spacings in order to also measure the rate of diffusion of the various relaxation components The results and discussion show that there is great potential for the here debuted methodology to study realistic and heterogeneous porous samples, as well as address important questions pertaining to the structure, transport and function in a variety of microporous and mesoporous materials.

## Acknowledgments

This work was supported by the UCSB NSFMRSEC Program (DMR-1121053) and the 2011 NIH Innovator award awarded to SH. JMF acknowledges support by the Elings Prize Postdoctoral Fellowship in Experimental Science from the California Nanosystems Institute (CNSI). This project made use of the UCSB MRL Shared Experimental Facilities, which are supported by the MRSEC Program of the National Science Foundation under award NSF DMR 1121053; a member of the NSF-funded Materials Research Facilities Network (www.mrfn.org).

## References

1. Ellis R. Macromolecular crowding: an important but neglected aspect of the intracellular environment. Curr. Opin. Struct. Biol. 2001; 11:114–119. [PubMed: 11179900]
2. Kleinberg R. Pore size distributions, pore coupling, and transverse relaxation spectra of porous rocks. Magn. Reson. Imaging. 1994; 12:271–274. [PubMed: 8170317]
3. Song Y. Categories of coherence pathways for the CPMG sequence. J. Magn Reson. 2002
4. Song Y. Pore sizes and pore connectivity in rocks using the effect of internal field. Magn. Reson Imaging. 2001
5. Schmidt-Rohr K, Chen Q. Parallel cylindrical water nanochannels in Nafion fuel-cell membranes. Nat. Mater. 2008; 7:75–83. [PubMed: 18066069]
6. Zhao Q, Majsztrik P, Benziger J. Diffusion and interfacial transport of water in Nafion. J. Phys. Chem. B. 2011; 115:2717–2727. [PubMed: 21370837]
7. Hickner, MMa. Ion-containing polymers: new energy & clean water. Materials Today. 2010; 13:34–41.
8. Aleksandrova E, Hink S, Hiesgen R, Roduner E. Spatial distribution and dynamics of proton conductivity in fuel cell membranes: potential and limitations of electrochemical atomic force microscopy measurements. Journal of physics. Condensed matter : an Institute of Physics journal. 2011; 23:234109. [PubMed: 21613704]
9. Callaghan PT. Rheo-NMR: nuclear magnetic resonance and the rheology of complex fluids. Reports on Progress in Physics. 1999; 62:599–670.
10. Callaghan PT, Coy A, MacGowan D, Packer KJ, Zelaya FO. Diffraction-like effects in NMR diffusion studies of fluids in porous solids. Nature. 1991; 351:467–469.
11. Aguayo JB, Blackband SJ, Schoeniger J, Mattingly MA, Hintermann M. Nuclear magnetic resonance imaging of a single cell. Nature. 1986; 322:190–191. [PubMed: 3724861]
12. Lee SC, Kim K, Kim J, Lee S, Han Yi J, Kim SW, Ha KS, Cheong C. One micrometer resolution NMR microscopy. J. Magn. Reson. 2001; 150:207–213. [PubMed: 11384182]
13. Ciobanu L, Seeber D, Pennington C. 3D MR microscopy with resolution by by. J. Magn. Reson. 2002; 158:178–182. [PubMed: 12419685]
14. Kleinberg R. Pore size distributions, pore coupling, and transverse relaxation spectra of porous rocks. Magn. Reson. Imaging. 1994; 12:271–274. [PubMed: 8170317]
15. Song Y-Q, Venkataramanan L, Hürlimann MD, Flaum M, Frulla P, Straley C. T(1)–T(2) correlation spectra obtained using a fast two-dimensional Laplace inversion. J. Magn. Reson. 2002; 154:261–268. [PubMed: 11846583]
16. Hürlimann M, Venkataramanan L. Quantitative Measurement of Two-Dimensional Distribution Functions of Diffusion and Relaxation in Grossly Inhomogeneous Fields. J. Magn. Reson. 2002; 157:31–42. [PubMed: 12202130]
17. Washburn K, Callaghan P. Tracking Pore to Pore Exchange Using Relaxation Exchange Spectroscopy. Phys. Rev. Lett. 2006; 97:25–28.

18. Song Y-Q, Venkataramanan L, Burcaw L. Determining the resolution of Laplace inversion spectrum. J. Chem. Phys. 2005; 122:104104. [PubMed: 15836306]
19. Lesage A, Lelli M, Gajan D, Caporini MA, Vitzthum V, Miéville P, Alauzun J, Roussey A, Thieuleux C, Mehdi A, Bodenhausen G, Copéret C, Emsley L. Surface enhanced NMR spectroscopy by dynamic nuclear polarization. J. Am. Chem. Soc. 2010; 132:15459–15461. [PubMed: 20831165]
20. Armstrong BD, Lingwood MD, McCarney ER, Brown ER, Blümler P, Han S. Portable X-band system for solution state dynamic nuclear polarization. J. Magn. Reson. 2008; 191:273–281. [PubMed: 18226943]
21. Armstrong BD, Han S. Overhauser dynamic nuclear polarization to study local water dynamics. J. Am. Chem. Soc. 2009; 131:4641–4647. [PubMed: 19290661]
22. McCarney ER, Armstrong BD, Lingwood MD, Han S. Hyperpolarized water as an authentic magnetic resonance imaging contrast agent. Proc. Natl. Acad. Sci. 2007; 104:1754–1759. [PubMed: 17264210]
23. Lingwood MD, Siaw TA, Sailasuta N, Abulseoud OA, Chan HR, Ross BD, Bhattacharya P, Han S. Hyperpolarized Water as an MR Imaging Contrast Agent: Feasibility of in Vivo Imaging in a Rat Model. Radiology. 2012; 265:418–425. [PubMed: 22996746]
24. Hürlimann MD, Griffin DD. Spin dynamics of Carr-Purcell-Meiboom-Gill-like sequences in grossly inhomogeneous B(0) and B(1) fields and application to NMR well logging. J. Magn Reson. 2000; 143:120–135. [PubMed: 10698653]
25. Hausser KH, Stehlik D. Dynamic nuclear polarization in liquids. Adv. Magn. Reson. 1968; 3:79–139.
26. Franck JM, Pavlova A, Han S. Quantitative cw Overhauser DNP Analysis of Hydration Dynamics. 2012:25. arxiv:1206.0510.
27. Armstrong BD, Choi J, López CJ, Wesener DA, Hubbell W, Cavagnero S, Han S. Site-Specific Hydration Dynamics in the Nonpolar Core of a Molten Globule by Dynamic Nuclear Polarization of Water. J. Am. Chem. Soc. 2011; 133:5987–5995. [PubMed: 21443207]
28. Pavlova A, McCarney ER, Peterson DW, Dahlquist FW, Lew J, Han S. Site-specific dynamic nuclear polarization of hydration water as a generally applicable approach to monitor protein aggregation. Phys. Chem. Chem. Phys. 2009; 11:6833–6839. [PubMed: 19639158]
29. McCarney ER, Armstrong BD, Kausik R, Han S. Dynamic nuclear polarization enhanced nuclear magnetic resonance and electron spin resonance studies of hydration and local water dynamics in micelle and vesicle assemblies. Langmuir : the ACS journal of surfaces and colloids. 2008; 24:10062–10072. [PubMed: 18700788]
30. Kausik R, Han S. Ultrasensitive detection of interfacial water diffusion on lipid vesicle surfaces at molecular length scales. J. Am. Chem. Soc. 2009; 131:18254–18256. [PubMed: 19791740]
31. Ortony JH, Cheng C-Y, Franck JM, Kausik R, Pavlova A, Hunt J, Han S. Probing the hydration water diffusion of macromolecular surfaces and interfaces. New J. Phys. 2011; 13:015006.
32. Bacic G, Niesman M, Bennett H, Magin R, Swartz H, Baccaron G. Others, Modulation of water proton relaxation rates by liposomes containing paramagnetic materials. Magn. Reson. Med. 2005; 6:445–458. [PubMed: 3380005]
33. Conti F, Negro E, Di Noto V, Elger G, Berthold T, Weber S. Time-resolved ESR investigation on energy transfer processes in Nafion photochemistry. Int. J. Hydrogen Energy. 2011:1–9.

## Highlights

We have demonstrated a methodology that enhances the contribution of small populations to standard NMR relaxometry methods.

We have proposed a model for applying this methodology to realistic systems.

We discuss how this methodology could be applied to study transport in porous systems.

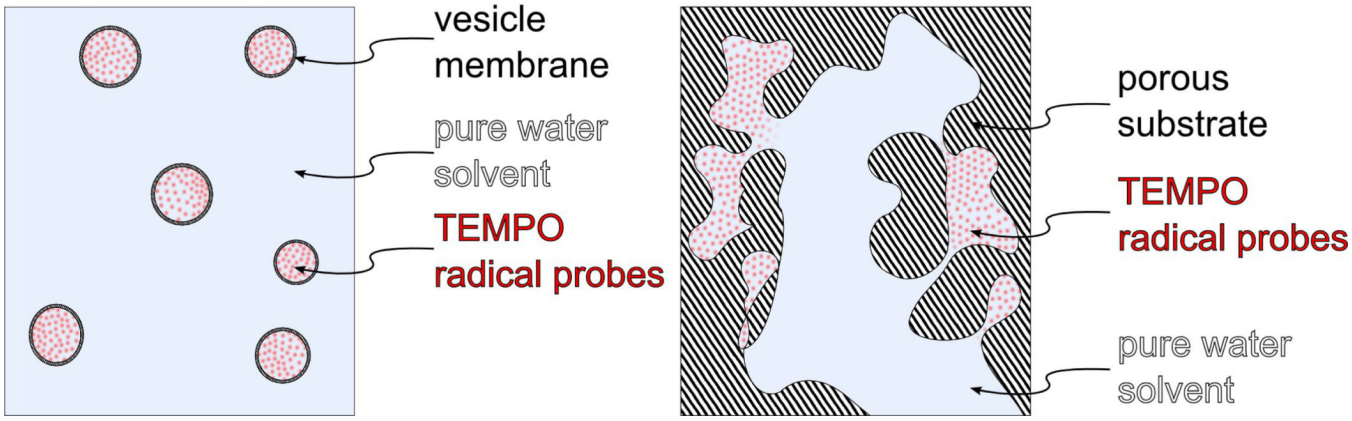


**Figure 1.**
Presents two possible applications of ODNP-amplified relaxometry. This technique could selectively resolve the dynamics or other properties of the water signal from inside lipid vesicle membranes (top), or from occluded water pockets within porous materials (bottom) that display only limited or slow exchange with the bulk water.

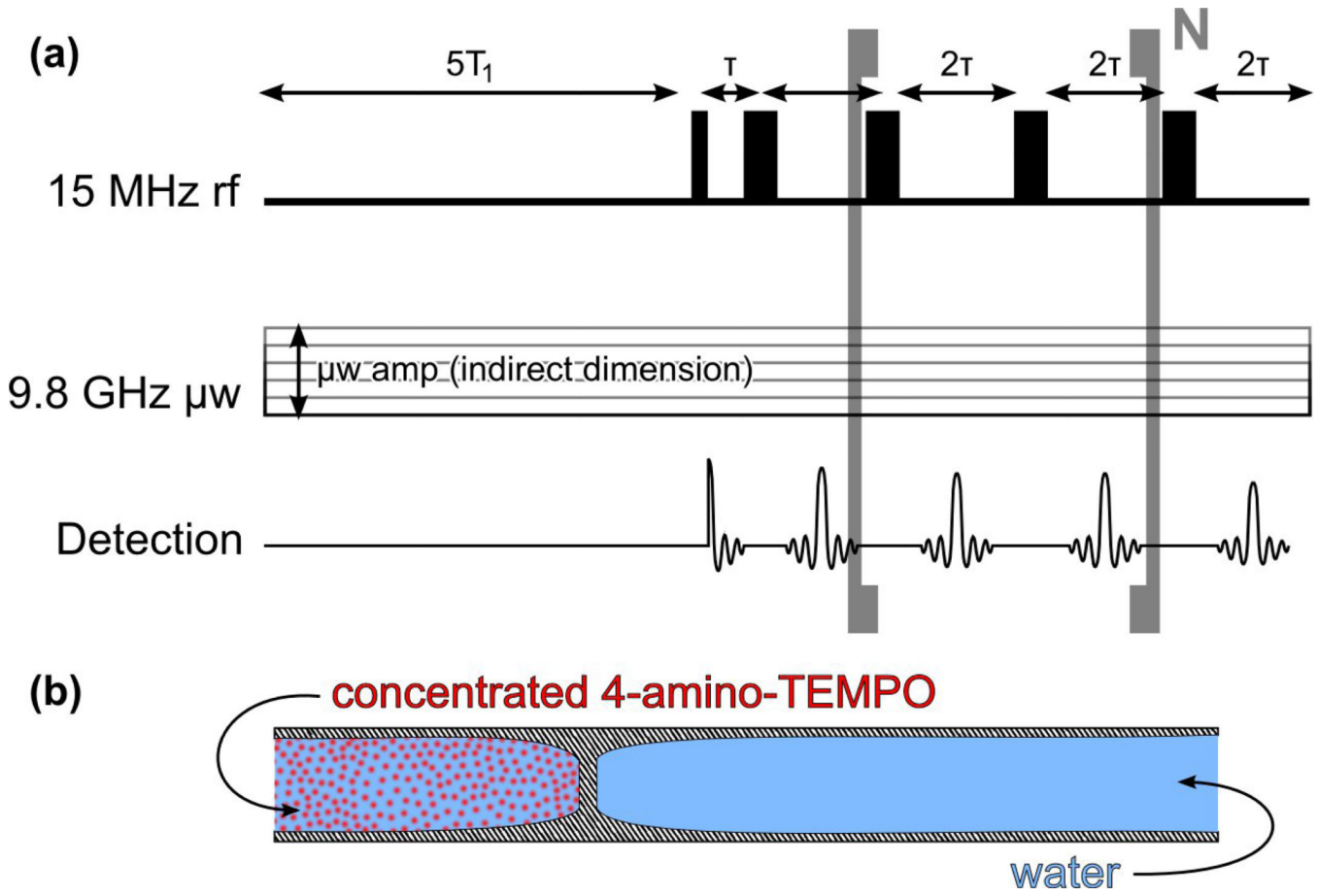


**Figure 2.**

Shows the CPMG pulse sequence used in this study (a) and the phantom sample (b) it was tested on. The bracketed portion of the pulse sequence, denoted by "N", repeats many times and maps out the $T_2$ relaxation decay. For the here presented data, the time $\tau$ is 3 ms and N=1000 echoes acquired in total. As indicated, the microwave power can vary continuously over a range of values, however, here, we present only slices along the indirect dimension at 0 and 2.5 mW of microwave power at 9.8 GHz. The phantom sample consists of a chamber containing pure water, and one where paramagnetic probe has been added, contained within a pinched 0.6 mm i.d. 0.84 mm o.d. quartz tube.

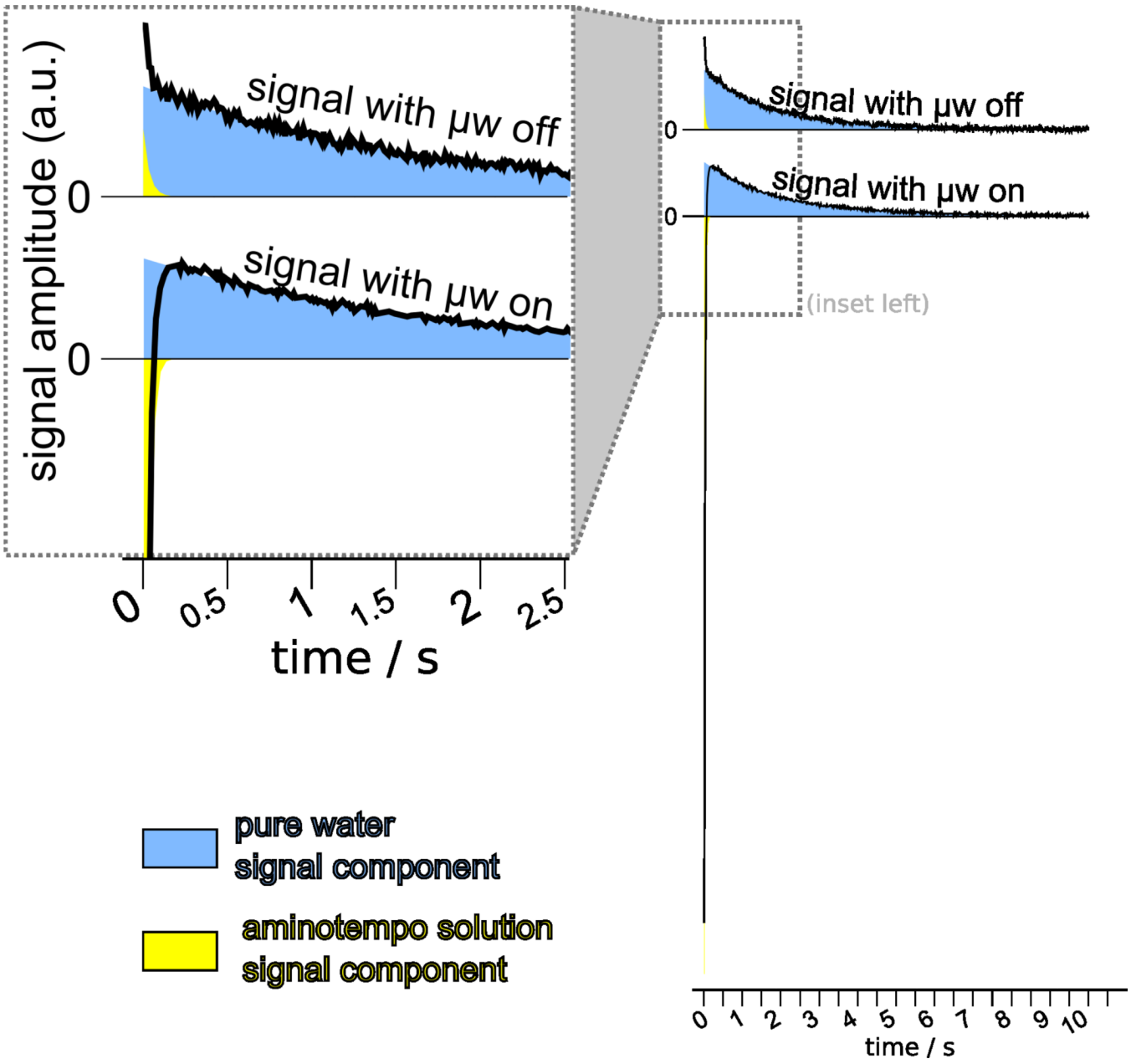


**Figure 3.**
Shows the NMR relaxometry (CPMG) signal acquired, both with and without irradiation with microwaves. The signal was generated by the phantom shown in fig. 2. The two components of a bi-exponential least-squares fit are plotted underneath for both signals. The saturating microwaves both invert and significantly enhance the rapidly relaxing and initially indistinguishable signal from the chamber containing the 100 mM 4-hydroxy-TEMPO probes

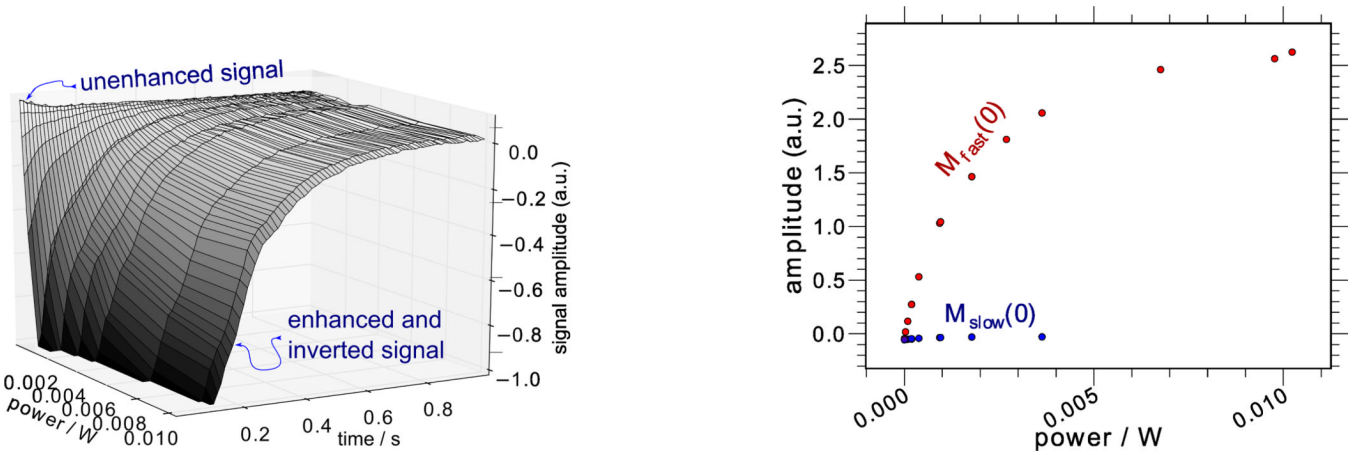


**Figure 4.**

Two-dimensional dataset, showing CPMG signal as a function of time (direct) and microwave power (indirect) dimensions. This data was acquired on a similar phantom as that of fig. 3, but with 14 mM, rather than 100 mM, 4-hydroxy-TEMPO (so that the fast-relaxing is slightly longer lived, allowing more facile biexponential fits). The unenhanced fast-relaxing signal and the enhanced fast-relaxing signal are indicated on the plot to the left, while the plot to the right provides the relative amplitudes of the two fit components for the amplitude, $M_{fast}(0)$ and $M_{slow}(0)$, of the faster and more slowly relaxing biexponential fits (which have time constants between 2–3 s and 12–18 ms), respectively. This data clearly shows saturation of the enhanced signal as the increasing microwave power saturates the ESR transition. For higher powers where the $M_s low(0)$ parameter is not plotted, the fast-relaxing, enhanced signal overwhelms the more slowly relaxing component, and the data is fit to a single exponential.